Published in final edited form as:
Ultrasound Med Biol. 2013 May ; 39(5): 893–902. doi:10.1016/j.ultrasmedbio.2012.11.017.

Toward Ultrasound Molecular Imaging with Phase-Change Contrast Agents: An In-Vitro Proof-of-Principle

Paul S. Sheeran[1,+], **Jason E. Streeter**[1,+], **Lee Mullin**[1], **Terry O. Matsunaga**[2], and **Paul A. Dayton**[1,*]

[1]Joint Department of Biomedical Engineering, The University of North Carolina and North Carolina State University, Chapel Hill, NC 27599, USA

[2]Department of Radiology Research, University of Arizona, Tucson, AZ 85724, USA

Abstract

Phase-change contrast agents (PCCAs), which normally consist of nano/microscale droplets of liquid perfluorocarbons (PFCs) in an encapsulating shell, can be triggered to undergo a phase transition to the highly-echogenic gaseous state upon the input of sufficient acoustic energy. As a result of the subsequent volumetric expansion, a number of unique applications have emerged that are not possible with traditional ultrasound microbubble contrast agents. Although many studies have explored the therapeutic aspects of the PCCA platform, few have examined the potential of PCCAs for molecular imaging purposes. In this study, we demonstrate a PCCA-based platform for molecular imaging using $\alpha_v\beta_3$-targeted nanoscale PCCAs composed of low-boiling-point PFCs. In-vitro, nanoscale PCCAs adhered to target cells, could be activated and imaged with a clinical ultrasound system and produced a six-fold increase in image contrast compared to non-targeted control PCCAs and a greater than fifty-fold increase over baseline. Data suggest that low-boiling-point nanoscale PCCAs could enable future ultrasound-based molecular imaging techniques in both the vascular and extravascular space.

Keywords

perfluorocarbon droplet; acoustic droplet vaporization; molecular imaging; contrast agent; phase-change

Introduction

Ultrasound Molecular Imaging

Contrast-enhanced ultrasonography based on microbubble contrast agents (MCAs) is a promising field with a wide range of applications for diagnostic and therapeutic purposes (Hernot and Klibanov 2008; Qin et al. 2009; Stride and Coussios 2010; Staub et al. 2010). By modifying the lipid, albumin, or polymer shell encapsulating typical MCAs to contain specific, high-affinity targeting ligands, a number of preclinical studies have demonstrated

*Corresponding Author, padayton@bme.unc.edu, Address: 304 Taylor Hall, CB 7575, Chapel Hill, NC 27599, Phone: (919) 843-9521, Fax: (919) 843-9520.
+These authors contributed equally to this work

the feasibility of using ultrasound molecular imaging (USMI) to detect cardiovascular disease, angiogenesis of solid tumors, inflammation processes, atherosclerosis, and thrombus (Klibanov 2006; Deshpande et al. 2009; Voigt 2009).

However, there are some fundamental limits and confounding factors involved with USMI based on MCAs. First, the perfluorocarbon (PFC) gas-core MCAs typically have low stability in circulation and dissolve into the surrounding media quickly. This, in combination with passive and active clearance by the lungs and mononuclear phagocyte system, results in a rapid elimination of contrast-providing agents over the course of several minutes (Mullin et al. 2011). Typical USMI schemes rely on measuring accumulation of a generally low number of targeted agents over time after a sufficient 'wait time' that allows for clearance of non-targeted, circulating agents (Gessner and Dayton 2010). Second, the size of MCAs that maximizes contrast once targeted (typically >1 μm in diameter (Streeter et al. 2010)) limits the MCAs to flow within the vascular space after injection. As a result, they are designed solely to target vascular diseases, such as inflammation, or intravascular markers that are indicators of processes beyond the vascular space, such as angiogenesis resulting from solid tumor growth (Figure 1a). Many approaches to molecular imaging and drug delivery in other modalities have exploited the enhanced permeability and retention effect of 'leaky' solid tumor vasculature to gradually accumulate particles on the order of 100 nm in the extravascular space via passive diffusion (Mulder et al. 2006). Though efforts have been made to generate targeted MCAs in sizes small enough to potentially diffuse beyond the vascular space and be registered by ultrasound imaging (Wang et al. 2011a), the reduced scattering cross-section of these particles (Quaia 2005) in combination with a resonance frequency much greater than those used for human diagnostic imaging (Sassaroli and Hynynen 2005) will significantly decrease the contrast provided. Furthermore, microbubbles with sizes on the order of 100s of nanometers are prone to collapse due to increasing Laplace pressures, which makes stabilizing such small bubbles challenging.

Phase-Change Contrast Agents

Several alternatives to MCAs exist for USMI. Contrast agents based on liquid perfluorocarbon nanodroplets have been proposed because as they exhibit some echogenicity (though inherently less than microbubbles) and are more stable in circulation than MCAs (Mattrey 1989; Behan et al. 1993; Hall et al. 2000; Marsh et al. 2002; Lanza et al. 2010). The more recent concept of acoustically activated phase-change contrast agents (PCCAs) has gained attention for diagnostic and therapeutic ultrasound (Kripfgans et al. 2000; Sheeran and Dayton 2012a). These agents are typically composed of PFCs that have boiling points close to body temperature, such as dodecafluoropentane (boiling point, 28–30°C) and perfluorohexane (boiling point, 58–60°C) (Kripfgans et al. 2000; Giesecke and Hynynen 2003; Fabiilli et al. 2009). Although they begin as liquid PFC droplets, they can be 'tipped' into the gaseous state by sufficient acoustic energy, or through heat-based effects. The resulting expansion in volume leads to a gas bubble 4–10 times the original diameter by ideal gas law predictions in combination with surface tension effects, and depending on initial droplet size and environmental conditions (Evans et al. 2006; Sheeran et al. 2011a). For the purposes of particles capable of extravasation, PCCAs present a unique advantage for ultrasound, in that particles in the liquid state can be generated at sizes small enough to extravasate, but become highly echogenic bubbles upon activation (Rapoport et al. 2009; Sheeran et al. 2011a). While the contrast provided by activated PCCAs has been demonstrated in several investigations (Kripfgans et al. 2000; Kripfgans et al. 2002), few studies have explored the potential of PCCAs as diagnostic agents for USMI.

One challenge in designing diagnostic and molecular imaging PCCAs at the microscale and nanoscale stems from the increase in surface tension effects. The Laplace pressure exerted on the core of PFC droplets as a result of surface tension scales with the inverse of the

particle's radius, and thus particles at the nanoscale can experience several atmospheres of additional pressure (Rapoport et al. 2009; Sheeran et al. 2011a). Because a compound's boiling point increases with increasing pressure (by the Clausius-Clapeyron relation), this results in a significantly increased 'effective boiling point' for the compound, which increases the ultrasound energy needed to vaporize the droplet. Several studies have shown that, as a result of this effect, microscale droplets can remain stable at temperatures up to 40°C above their bulk boiling point, although they can still be vaporized with diagnostically relevant acoustic parameters (Giesecke and Hynynen 2003; Fabiilli et al. 2009; Martz et al. 2011). Nanoscale PCCAs of the typically-used PFCs, on the other hand, may require acoustic parameters only suitable for therapeutic purposes (Zhang and Porter 2010; Sheeran et al. 2011a). A recent study by Wang and colleagues demonstrated active PCCA targeting to cancer cells *in vitro* through aptamer-conjugated droplets of dodecafluoropentane – the most commonly used perfluorocarbon for PCCAs (Wang et al. 2011b). As a result of the significant pressures needed to induce phase-transition, the authors observed mechanical cell destruction coinciding with vaporization. While this result may be a desirable result for therapeutic/drug delivery applications, a non-invasive imaging approach should avoid the likelihood of bioeffects.

Generating PCCAs from Low-Boiling-Point PFCs

The ability to create sub-micron PCCAs with low vaporization thresholds has been recently demonstrated through formulation using very low-boiling-point PFCs such as decafluorobutane (DFB, boiling point −1.1 to −2°C), octafluoropropane (boiling point −36.7°C), and as well as mixtures of each (Sheeran et al. 2011a; Sheeran et al. 2011b; Sheeran et al. 2012b). This is accomplished by exploiting the 'bi-stable' nature of the particles created by the influence of Laplace pressure; at larger sizes the internal pressure is much less and the particles prefer the gaseous state, whereas at very small sizes the internal pressure is very high – hence a greatly increased 'effective boiling point' – and the particles will remain stable in the liquid state well above their atmospheric pressure boiling point (Rapoport et al. 2009; Sheeran et al. 2011a). This property has also resulted in the development of a simple, high-yield technique of 'microbubble condensation' to generate microscale and nanoscale PCCAs from compounds that are normally a gas at room temperature (Sheeran et al. 2011b). In preliminary demonstrations, it has been observed that this method is effective for creating DFB droplets with diameters in the 200–400 nm range, and that the DFB droplets have significantly reduced vaporization thresholds compared to droplets composed of more commonly used PFCs (such as perfluoropentane) as a result of the greatly-decreased boiling point. DFB droplet samples were shown to remain stable in distribution and concentration for periods greater than 1 hour once exposed to physiologic temperatures (Sheeran et al. 2012b), which is promising for *in vivo* applications requiring accumulation of circulating agents.

One of the primary benefits of the microbubble condensation technique is that it allows for simple modification of droplet properties (size, composition) by altering the precursor MCAs through well-described methods. Nanodroplets capable of USMI or gene delivery can be generated by first preparing MCAs containing targeting ligands or gene vectors and then condensing to the droplet form. PCCAs generated via this method have the potential to be made in sizes small enough to extravasate into the tumor interstitium and target specific cell markers, and then be activated to form echogenic MCAs and be registered through ultrasound imaging (Figure 1B). Even as purely intravascular agents, PCCAs may have benefits in reducing the 'wait time' needed to obtain imaging contrast. Once a sufficient number of droplets have accumulated at the vascular site of interest, an activation pulse may be delivered to vaporize the agents in a desired location (Figure 1C). The remaining non-activated droplets still in circulation will have very little contrast relative to the highly

echogenic targeted bubbles, and so information on molecular expression may be gathered more quickly.

In this study, we explore *in vitro* the feasibility of using PCCAs derived from low-boiling-point PFCs as USMI agents. We demonstrate that targeting ligands can be simply incorporated into the encapsulating shell of the precursor microbubbles, and that the resulting droplets successfully target cellular markers of angiogenesis (such as $\alpha_v\beta_3$). Furthermore, the main benefit using low-boiling-point PFCs is demonstrated by activating targeted droplets using a clinical diagnostic ultrasound machine while maintaining the adhesion of the resultant microbubble to the cellular marker.

Methods

Microbubble Preparation

All lipid solutions consisted of 1,2-distearoyl-*sn*-glycero-3-phosphocholine (DSPC), 1,2-distearoyl-sn-glycero-3-phosphoethanolamine-N-methoxy(polyethylene-glycol)-2000 (DSPE-PEG2000), and 1,2-distearoyl-sn-glycero-3-phosphoethanolamine-N-maleimide(polyethylene-glycol)-2000 (DSPE-MALPEG2000), in a 9:0.5:0.5 molar ratio, respectively, with a total lipid concentration of 1.0 mg/mL (Avanti Polar Lipids, Alabaster, AL). To create a particle designed to target $\alpha_v\beta_3$ integrins, a cyclic RGD peptide (Cyclo-Arg-Gly-Asp-D-Tyr-Cys) cross-linked to DSPE-MAL-PEG2000 was included similar to previous studies by our group (Streeter et al. 2010). Similarly, non-targeted (sham control) particles were created using a cyclic RAD peptide (Cyclo-Arg-Ala-Asp-D-Tyr-Cys) cross-linked to DSPE-MAL-PEG2000 that is known to not target $\alpha_v\beta_3$ integrins. The cyclic RAD and RGD peptides were purchased from Peptides International (Louisville, KY). The excipient solution was comprised of phosphate-buffered saline (PBS), propylene glycol, and glycerol (16:3:1) for a total lipid concentration of 1.0 mg/mL. After adding 1.5 mL of the resulting solution to a 3 mL glass vial, the headspace of the vial was gas-exchanged with decafluorobutane (Fluoromed, Round Rock, TX). MCAs were formed via standard mechanical agitation techniques using a Vialmix shaker (Bristol-Myers-Squibb, New York, NY).

Microbubble Condensation

MCA samples were condensed using a protocol from previous studies (Sheeran et al. 2011b). Briefly, the 3 mL vials containing DFB MCAs were submerged in a CO_2/isopropanol bath, controlled to a temperature between −5°C and −10°C, and swirled gently for 1 minute. A 30 mL syringe filled with room-air was connected to the vial using a 25 G needle through the septum, and the plunger was depressed using a mechanical system until headspace pressure reached approximately 5–10 psi and a change in consistency was noted in the sample – indicating the onset of condensation. Throughout this procedure, the vial was gently swirled and observed periodically to ensure the lipid solution did not freeze due to the low temperatures used. After condensation, the syringe needle was removed from the vial, leaving a slight pressure head on the solution.

Sample Sizing

Targeted and non-targeted MCA size distributions were measured using an Accusizer 780 (Particle Sizing Systems, Santa Barbara, CA) capable of measuring particles as small as 0.5 μm in diameter. Accusizer sample volumes were typically 3 μL for bubble samples. Dynamic light scattering (Malvern Nano ZS, Malvern Instruments Ltd., Malvern, Worcestershire, U.K.) was employed to characterize droplet distributions after condensation. Approximately 1 to 1.5 mL of each condensed droplet sample was transferred to a cuvette

and the size distribution of the sample measured 3 times and averaged. The Malvern Nano ZS was capable of measuring particles as large as 6 μm in diameter.

Cell Culture

Human umbilical vein endothelial cells (HUVEC) (CC-2519) were cultured in Endothelial Cell Basal Medium-2 (EBM-2; CC-3156) supplemented with EGM-2 SingleQuot Kit Suppl. & Growth Factors (CC-4176) (Lonza, Walkersville, MD). HUVEC in culture have been previously shown to overexpress the $\alpha_v\beta_3$ integrin (Dayton et al. 2004). Cells were maintained in a humidified atmosphere containing 5% CO_2 at 37 °C, and were grown in a monolayer on nearly acoustically transparent Thermanox™ slips (Nalge Nunc International, Rochester, NY) coated with 2% gelatin.

When cells reached 80–90% confluence they were incubated for 15 minutes with 100 μL of the droplet solution diluted in 3 mL of media. After incubation, the cover slips were rigorously washed with media by flushing at 3 mL syringe over the coverslip at a rate of approximately 0.5 mL/second and then samples were placed in a metal holder. A media-filled fluid pocket was created with a gasket and Thermanox™ cover slip opposite the glass cover slip (Figure 2).

Microscopy

Brightfield images were obtained at two time-points: just after the cell/PCCA sample incubation period, and just after cell exposure to ultrasound. In order to capture microscope images after ultrasonic imaging, the fluid pocket formed by the gasket and dual Thermanox™ slips was taken apart and the lower coverslip submerged in a 6-well plate with 3 mL of PBS. All images were captured using a 60X immersion objective (NA=1.0) with a BX51 Microscope (Olympus, Center Valley, PA) and Metamorph Basic software (Molecular Devices, Sunnyvale, CA).

Experimental Apparatus

Ultrasound imaging of each sample was performed with a Siemens Sequoia Imaging System (Acuson Sequioa 512) with a 15L8 linear array transducer positioned at an angle relative to the sample (as shown in Figure 3) to minimize specular reflections back towards the transducer. The transducer was placed in a clamp that was mounted to a 2-D motion stage with the ability to elevationally control the transducer position using a custom LabVIEW (LabVIEW, National Instruments Corp., Austin, TX) program for the goal of generating volumetric data. Samples contained in the metal holder were placed in a plastic-lined degassed water-bath at body temperature (37°C) using acrylic stand-offs to adjust the height relative to the transducer. The focal point of the transducer was set to the axial position of the cell sample located on the Thermanox™ cover slip. Volumetric B-mode scans were acquired for overlays and drawing regions of interest using the system's compounding mode (Freq: 14 MHz, Mechanical Index (MI): 0.1) while stepping the transducer at 0.4 mm increments across the cover slip. The elevational beamwidth was previously determined to be 0.8 mm (Thijssen et al. 2007, Feingold et al. 2010). Similarly, baseline volumetric Cadence™ pulse sequencing (CPS) scans (Freq: 7 MHz, MI: 0.18, CPS Gain: −20dB) were acquired with elevational increments of 0.4 mm stepped across the sample. To vaporize targeted and non-targeted droplets present in the samples, the system was set to B-mode with a MI of 1.1 and a frequency of 8 MHz while the transducer was elevationally translated at 1 mm/s across the sample with an imaging frame rate of 30 Hz. These acoustic parameters were chosen based on prior *in vitro* work demonstrating that 2–3 cycle imaging pulses (such as those delivered by the Sequoia) with mechanical indices of 1 or higher are sufficient to cause DFB droplet vaporization (Sheeran et al. 2011b; Sheeran et al. 2012b). After exposure to the higher pressure, the sample was rescanned in CPS mode (Freq: 7 MHz, MI: 0.18, CPS

Gain: −20dB) to capture the increase in contrast from the newly formed bubbles. All other ultrasound parameters (such as gain and time-gain compensation) were kept constant between samples.

Data Analysis

Contrast enhancement was measured using the Siemens Sequoia CPS mode where the mean pixel intensities of the volumetric data were assumed to be proportional to the degree of molecular biomarker expression. Regions of interest were manually drawn around the perimeter of the cover slip boundaries in each image plane using the previously acquired B-mode image data. With custom MATLAB (The Mathworks, Natick, MA) scripts, the volumetric intensities for each cover slip were obtained by summing all of the pixel intensity values for each voxel within the drawn regions of interest and dividing that value by the total number of voxels within the volume. For each targeted (N = 6) and non-targeted (N = 6) experiment, mean volumetric intensities from pre- and post-vaporization images were calculated to yield a final volumetric measure of $\alpha_v\beta_3$ targeting. Significance between compared distributions was analyzed in Excel using a two-sided student's t-test with equal variance. The significance between the different distributions was considered at a value of $p < .05$. Images were created by setting the acquired CPS intensity data to a green-scale of 0 to 256 and creating overlays of the CPS and B-mode data.

Results

In these results, we demonstrate the feasibility of using low-boiling-point PCCAs for diagnostic USMI by comparing the *in vitro* contrast enhancement provided after incubating targeted samples with $\alpha_v\beta_3$-expressing HUVECs and inducing vaporization with a clinical diagnostic ultrasound machine.

Sample Sizing

Targeted and non-targeted samples had similar distributions in both the precursor MCA stage and the condensed droplet stage. The originating cyclic RGD (targeted) and cyclic RAD (non-targeted) MCA samples had mean diameters of 1.07 ± 0.78 μm and 1.09 ± 0.94 μm, respectively (Figure 3a). The condensed droplets typically formed peaks at 295 nm in diameter with a wide distribution through the nanoscale range (Figure 3b), including the presence of outlier microscale droplets resulting from bubbles greater than 5 μm present in the original MCA distribution.

Ultrasonic Vaporization and Microscopy

To demonstrate the feasibility of USMI with low-boiling-point PCCAs, a total of 12 plated HUVEC samples expressing $\alpha_v\beta_3$ were incubated with targeted (N=6) and non-targeted (N=6) droplet samples and then imaged by a Siemens Sequoia. Activation pulses over the coverslip length took approximately 20 seconds, and the ultrasound imaging scan was taken within 30 seconds of the final activation pulse. After the imaging data was captured (approximately 50 seconds), 2–3 minutes elapsed while samples were transferred to the microscope. Both contrast-specific ultrasound CPS scans and microscopy results suggest that very few bubbles were present prior to the activation pulse for both targeted and non-targeted samples, indicating that any targeted particles were likely still in the condensed liquid state (low echogenicity) after the incubation period (Figures 4a, 5a). In the microscopy images, the presence of outlier microscale droplets could be observed in targeted samples, although nanoscale droplets were not optically resolvable (Figure 5a).

After the HUVEC cell samples were exposed to the activation pulse (mechanical index of 1.1 at 8 MHz), samples that were incubated with targeted droplets showed the presence of

newly-created regions of high contrast (many that maximized the CPS signal) - indicating the presence of highly echogenic bubbles not previously there (Figure 4b). This was confirmed by microscopy, where only slides incubated with targeted droplets showed a significant presence of still-adherent bubbles (Figure 5b), although many bubbles became detached and were lost in the process of dis-assembling the fluid pocket and re-submerging the cell-bearing coverslip in the 6-well plates for microscope imaging.

Throughout the course of the tests, a small degree of non-selective droplet targeting was observed for samples incubated with cyclic RAD droplets that resulted in ultrasound contrast. This was also confirmed by the presence of occasional microscale droplets (before the vaporization pulse) and MCAs (after the vaporization pulse) on these samples in microscopy images, although a significantly smaller number than present for targeted samples.

Ultrasound scans were taken across the cell samples at elevational increments of 0.4 mm for a total of 41 ultrasound 'slices' per sample before and after exposure to the activation pulse. Rendering the ensemble of slices in 3D allows for visualization of the volumetric data (Figure 6) – revealing the drastic difference in contrast enhancement provided by $\alpha_v\beta_3$-targeting droplets as well as the spatial variation in the targeting/activation across the cell plates. As the elevational resolution of the transducer is approximately 0.8 mm at 7 MHz (Thijssen et al. 2007, Feingold et al. 2010), each intermediate image was discarded from the dataset to ensure no overlap in data between slices, resulting in a total of 20 volumetric slices per sample for data analysis. Over the 6 cell samples tested for each group (targeted, non-targeted), the ultrasound data showed a mean intensity of approximately 19.0 ± 11.8 arbitrary units for samples incubated with targeted droplets (N=6), and a mean intensity of approximately 3.3 ± 3.9 arbitrary units for non-targeted droplets (N=6) (Figure 7). The post-vaporization data was statistically significant over baseline for targeted samples ($p=0.01$), but not for non-targeted samples ($p=0.10$). The baseline scans were not statistically significant between targeted and non-targeted groups ($p=0.23$). Comparing the targeted to non-targeted data shows a statistically significant ($p=0.02$), nearly 6-fold increase in the mean image intensity (in dB).

Discussion

These results show proof-of-principle that PCCAs generated from low-boiling-point perfluorocarbons can be used as effective, dynamic USMI agents with unique properties compared to standard MCA-based USMI agents. To our knowledge, this is the first study, to date, that demonstrates diagnostic USMI with PCCAs where vaporization pulses were delivered from a clinical diagnostic ultrasound machine. The latter is primarily a result of the use of very low-boiling-point perfluorocarbons that require inherently less acoustic energy to vaporize than commonly-used PFCs such as dodecafluoropentane. In this study, a cyclic RGD peptide was incorporated into the encapsulating shell for the purpose of targeting cellular $\alpha_v\beta_3$ expression, although in future studies a number of alternative ligands could be selected to target specific disease states and incorporated in a simple method as demonstrated here.

Interestingly, the fact that the bubbles resulting from vaporized droplets remained strictly in the plane of the cells (rather than floating to the upper coverslip and showing as points of high contrast) strongly suggests that the encapsulating shell remained intact during vaporization, and that a significant portion of the bubbles did not become dislodged as a result of vaporization (Figure 4). This is further evidenced by the bubbles remaining adherent to cells after transfer to 6-well plates for microscopy (Figure 5). Whether the agents demonstrated here have 'excess' shell in the droplet state primarily as a result of the

microbubble condensation method, or whether retention of the encapsulating shell after vaporization is a property of all PCCA generation techniques will need to be explored in future studies. That the resulting bubbles do not dislodge during vaporization and remain adherent to the target sites is an important factor for PCCA-based USMI in ensuring that the contrast-providing bubbles are viable indicators of the underlying molecular processes. Additionally, the visible confluence of the cells did not appear to be altered by the activation, as would be expected if the cells became mechanically disrupted or dislodged during droplet vaporization, although more work is needed to explore whether more subtle interactions may be occurring.

In all experiments, the cell samples incubated with targeted droplets showed consistently higher mean pixel intensity than those incubated with non-targeted droplets. That some amount of non-selective binding occurs is consistent with both *in vitro* and *in vivo* results using MCA-based USMI agents (Lindner et al. 2000; Leong-Poi et al. 2003; Klibanov et al. 2006; Streeter et al. 2010; Streeter et al. 2011), and so future studies establishing the extent to which this also occurs for PCCAs will be important. Because this study investigated the general feasibility of using PCCAs as USMI agents, much work can be done to further optimize parameters. As with MCAs, careful study is needed to define the proper ‘wait time’ that balances agent deposition at the target site with clearance from the mononuclear phagocyte system and general agent instability. Additionally, the ideal ultrasound ‘activation’ signal would be one that uses the least amount of energy needed (to minimize unwanted bioeffects), and limits each droplet to only a few high-energy vaporization pulses (to minimize secondary effects such as coalescence, fragmentation) (Dayton et al. 1999; Chomas et al. 2001). In this study, droplets were exposed to approximately 15–20 pulses during the period the ultrasound transducer was translating over the sample volume. Although many small bubbles resulting from vaporization of nano-PCCAs were present (Figure 5b), coalescence due to repeated pulsing (Postema et al. 2004) may explain the presence of some large bubbles that were observed in the microscope images after vaporization (on the order of 15 – 25 μm in diameter). Though present in much smaller quantities than bubbles on the order of 1–5 μm in diameter, these large bubbles were likely major contributors to the total scattered ultrasound signal. It is also possible that these bubbles were a result of the larger outlier droplets present in the polydisperse samples. Although the diameter distribution peak was on the order of 295 nm, DLS measurements (Figure 3) and microscopy (Figure 5a) both show presence of a small amount of droplets on the order of 1–3 μm, which could vaporize to form bubbles on this order. In this study, the intent was to investigate the general feasibility of a PCCA-based platform for molecular imaging. However, refinement in the broad size distribution used here is needed depending on whether molecular imaging is aimed at the intravascular space or extravascular space. For extravascular USMI, targeted emulsions should ideally have droplets on the order of 100–300 nm to enable extravasation, whereas vascular targeting could be accomplished with droplets much larger.

Conclusion

Ultrasound-based molecular imaging with phase-change contrast agents presents a promising new set of tools for detecting both intravascular and extravascular cellular markers. Through the microbubble condensation technique, nanoscale PCCAs with both high stability in biological media and inherently high sensitivity to ultrasound can be generated with a wide variety of targeting ligands to detect disease-specific markers *in vitro* and *in vivo*. One of the most unique aspects of a PCCA-based molecular imaging approach is that the imaging modality – ultrasound – allows for real-time spatial and temporal specificity of the agent activation and the subsequent imaging. Our demonstration suggests that targeted PCCAs can be designed to target cell-surface receptors. Furthermore, continued

adhesion to the receptor following activation provides strong evidence that the avidity of both the PCCA and the resultant microbubble to the receptor is significantly robust to allow for selective molecular imaging to cell surface markers.

Acknowledgments

This work was supported by NIH grants no. R21EB011704 (Matsunaga) and R01EB009066 (Dayton and Borden), and pilot study funds from UNC Chapel Hill. The authors acknowledge Professor Mark Borden at the University of Colorado for insightful discussions regarding microbubble condensation. P.S. appreciates the generous support of the National Science Foundation as the recipient of a graduate fellowship.

References

Behan M, O'Connell D, Mattrey R, Carney D. Perfluorooctylbromide as a contrast agent for CT and sonography: preliminary clinical results. Am J Roentgenol. 1993; 160:399–405. [PubMed: 8424361]

Chomas JE, Dayton P, May D, Ferrara K. Threshold of fragmentation for ultrasonic contrast agents. J Biomed Opt. 2001; 6:141–150. [PubMed: 11375723]

Dayton PA, Morgan KE, Klibanov AL, Brandenburger GH, Ferrara KW. Optical and acoustical observations of the effects of ultrasound on contrast agents. IEEE Trans Ultrason Ferroelectr Freq Control. 1999; 46:220–232. [PubMed: 18238417]

Dayton PA, Pearson D, Clark J, Simon S, Schumann PA, Zutshi R, Matsunaga TO, Ferrara KW. Ultrasonic analysis of peptide- and antibody-targeted microbubble contrast agents for molecular imaging of αvβ3-expressing cells. Mol Imaging. 2004; 3:125–134. [PubMed: 15296677]

Deshpande N, Needles A, Willmann JK. Molecular ultrasound imaging: current status and future directions. Clin Radiol. 2009; 65:567–581. [PubMed: 20541656]

Evans DR, Parsons DF, Craig VS. Physical properties of phase-change emulsions. Langmuir. 2006; 22:9538–9545. [PubMed: 17073477]

Fabiilli ML, Haworth KJ, Fakhri NH, Kripfgans OD, Carson PL, Fowlkes JB. The role of inertial cavitation in acoustic droplet vaporization. IEEE Trans Ultrason Ferroelectr Freq Control. 2009; 56:1006–1017. [PubMed: 19473917]

Feingold S, Gessner R, Guracar IM, Dayton PA. Quantitative volumetric perfusion mapping of the microvasculature using contrast ultrasound. Invest Radiol. 2010; 45:669–674. [PubMed: 20808232]

Gessner R, Dayton PA. Advances in molecular imaging with ultrasound. Mol Imaging. 2010; 9:117–127. [PubMed: 20487678]

Giesecke T, Hynynen K. Ultrasound-mediated cavitation thresholds of liquid perfluorocarbon droplets in vitro. Ultrasound Med Biol. 2003; 29:1359–1365. [PubMed: 14553814]

Hall CS, Lanza GM, Rose JH, Kaufmann RJ, Fuhrhop RW, Handley SH, Waters KR, Miller JG, Wickline SA. Experimental determination of phase velocity of perfluorocarbons: applications to targeted contrast agents. IEEE Trans Ultrason Ferroelectr Freq Control. 2000; 47:75–84. [PubMed: 18238519]

Hernot S, Klibanov AL. Microbubbles in ultrasound-triggered drug and gene delivery. Adv Drug Deliv Rev. 2008; 60:1153–1166. [PubMed: 18486268]

Klibanov AL. Microbubble contrast agents: targeted ultrasound imaging and ultrasound-assisted drug-delivery applications. Invest Radiol. 2006; 41:354–362. [PubMed: 16481920]

Klibanov AL, Rychak JJ, Yang WC, Alikhani S, Li B, Acton S, Lindner JR, Ley K, Kaul S. Targeted ultrasound contrast agent for molecular imaging of inflammation in high-shear flow. Contrast Media Mol Imaging. 2006; 1:259–266. [PubMed: 17191766]

Kripfgans OD, Fowlkes JB, Miller DL, Eldevik OP, Carson PL. Acoustic droplet vaporization for therapeutic and diagnostic applications. Ultrasound Med Biol. 2000; 26:1177–1189. [PubMed: 11053753]

Kripfgans OD, Fowlkes JB, Woydt M, Eldevik OP, Carson PL. In vivo droplet vaporization for occlusion therapy and phase aberration correction. IEEE Trans Ultrason Ferroelectr Freq Control. 2002; 49:726–738. [PubMed: 12075966]

Lanza G, Winter P, Caruthers S, Hughes MS, Hu G, Schmieder AH, Wickline SA. Theragnostics for tumor and plaque angiogenesis with perfluorocarbon nanoemulsions. Angiogenesis. 2010; 13:189–202. [PubMed: 20411320]

Leong-Poi H, Christiansen J, Klibanov AL, Kaul S, Lindner JR. Noninvasive assessment of angiogenesis by ultrasound and microbubbles targeted to alpha(v)-integrins. Circulation. 2003; 107:455–460. [PubMed: 12551871]

Lindner JR, Song J, Xu F, Klibanov AL, Singbartl K, Ley K, Kaul S. Noninvasive ultrasound imaging of inflammation using microbubbles targeted to activated leukocytes. Circulation. 2000; 102:2745–2750. [PubMed: 11094042]

Marsh JN, Hall CS, Scott MJ, Fuhrhop RW, Gaffney PJ, Wickline SA, Lanza GM. Improvements in the ultrasonic contrast of targeted perfluorocarbon nanoparticles using an acoustic transmission line model. IEEE Trans Ultrason Ferroelectr Freq Control. 2002; 49:29–38. [PubMed: 11833889]

Martz TM, Sheeran PS, Bardin D, Lee AP, Dayton PA. Precision Manufacture of Phase-Change Perfluorocarbon Droplets using Microfluidics. Ultrasound Med Biol. 37(11):1952–1957. [PubMed: 21963036]

Mattrey RF. Perfluorooctylbromide: a new contrast agent for CT, sonography, and MR imaging. Am J Roentgenol. 1989; 152:247–252. [PubMed: 2643258]

Mulder WJ, Strijkers GJ, van Tilborg GA, Griffioen AW, Nicolay K. Lipid-based nanoparticles for contrast-enhanced MRI and molecular imaging. NMR Biomed. 2006; 19:142–164. [PubMed: 16450332]

Mullin L, Gessner R, Kwan J, Kaya M, Borden MA, Dayton PA. Effect of anesthesia carrier gas on in vivo circulation times of ultrasound microbubble contrast agents in rats. Contrast Media Mol Imaging. 2011; 6:126–131. [PubMed: 21246710]

Postema M, Marmottant P, Lancee CT, Hilgenfeldt S, de Jong N. Ultrasound-induced microbubble coalescence. Ultrasound Med Biol. 2004; 30:1337–1344. [PubMed: 15582233]

Qin S, Caskey CF, Ferrara KW. Ultrasound contrast microbubbles in imaging and therapy: physical principles and engineering. Phys Med Biol. 2009; 54:R27–R57. [PubMed: 19229096]

Quaia, E., editor. Contrast media in ultrasonography: basic principles and clinical applications. New York: Springer; 2005.

Rapoport NY, Kennedy AM, Shea JE, Scaife CL, Nam KH. Controlled and targeted tumor chemotherapy by ultrasound-activated nanoemulsions/microbubbles. J Control Release. 2009; 138:268–276. [PubMed: 19477208]

Sassaroli E, Hynynen K. Resonance frequency of microbubbles in small blood vessels: a numerical study. Phys Med Biol. 2005; 50:5293. [PubMed: 16264254]

Sheeran PS, Dayton PA. Phase-change contrast agents for imaging and therapy. Curr Pharm Des. 2012a; 18:2152–2165. [PubMed: 22352770]

Sheeran PS, Luois S, Dayton PA, Matsunaga TO. Formulation and acoustic studies of a new phase-shift agent for diagnostic and therapeutic ultrasound. Langmuir. 2011b; 27:10412–10420. [PubMed: 21744860]

Sheeran PS, Luois S, Mullin L, Matsunaga TO, Dayton PA. Design of ultrasonically-activatable nanoparticles using low boiling point perfluorocarbons. Biomaterials. 2012b; 33:3262–3269. [PubMed: 22289265]

Sheeran PS, Wong VP, Luois S, McFarland RJ, Ross WD, Feingold S, Matsunaga TO, Dayton PA. Decafluorobutane as a phase-change contrast agent for low-energy extravascular ultrasonic imaging. Ultrasound Med Biol. 2011a; 37:1518–1530. [PubMed: 21775049]

Staub D, Schinkel AFL, Coll B, Coli S, van der Steen AF, Reed JD, Krueger C, Thomenius KE, Adam D, Sijbrands EJ, ten Cate FJ, Feinstein SB. Contrast-enhanced ultrasound imaging of the vasa vasorum: from early atherosclerosis to the identification of unstable plaques. J Am Coll Cardiol Img. 2010; 3:761–771.

Streeter JE, Gessner R, Miles I, Dayton PA. Improving sensitivity in ultrasound molecular imaging by tailoring contrast agent size distribution: in vivo studies. Mol Imaging. 2010; 9:87–95. [PubMed: 20236606]

Streeter JE, Gessner RC, Tsuruta J, Feingold S, Dayton PA. Assessment of molecular imaging of angiogenesis with three-dimensional ultrasonography. Mol Imaging. 2011; 10:460–468. [PubMed: 22201537]

Stride EP, Coussios CC. Cavitation and contrast: the use of bubbles in ultrasound imaging and therapy. Proc Inst Mech Eng H. 2010; 224:171–191. [PubMed: 20349814]

Thijssen JM, Weijers G, de Korte CL. Objective performance testing and quality assurance of medical ultrasound equipment. Ultrasound Med Biol. 2007; 33:460–471. [PubMed: 17275983]

Voigt JU. Ultrasound molecular imaging. Methods. 2009; 48:92–97. [PubMed: 19324089]

Wang CH, Huang YF, Yeh CK. Aptamer-conjugated nanobubbles for targeted ultrasound molecular imaging. Langmuir. 2011a; 27:6971–6976. [PubMed: 21553884]

Wang CH, Kang ST, Lee YH, Luo YL, Huang YF, Yeh CK. Aptamer-conjugated and drug-loaded acoustic droplets for ultrasound theranosis. Biomaterials. 2011b; 33:1939–1947. [PubMed: 22142768]

Zhang P, Porter T. An in vitro study of a phase-shift nanoemulsion: a potential nucleation agent for bubble-enhanced HIFU tumor ablation. Ultrasound Med Biol. 2010; 36:1856–1866. [PubMed: 20888685]

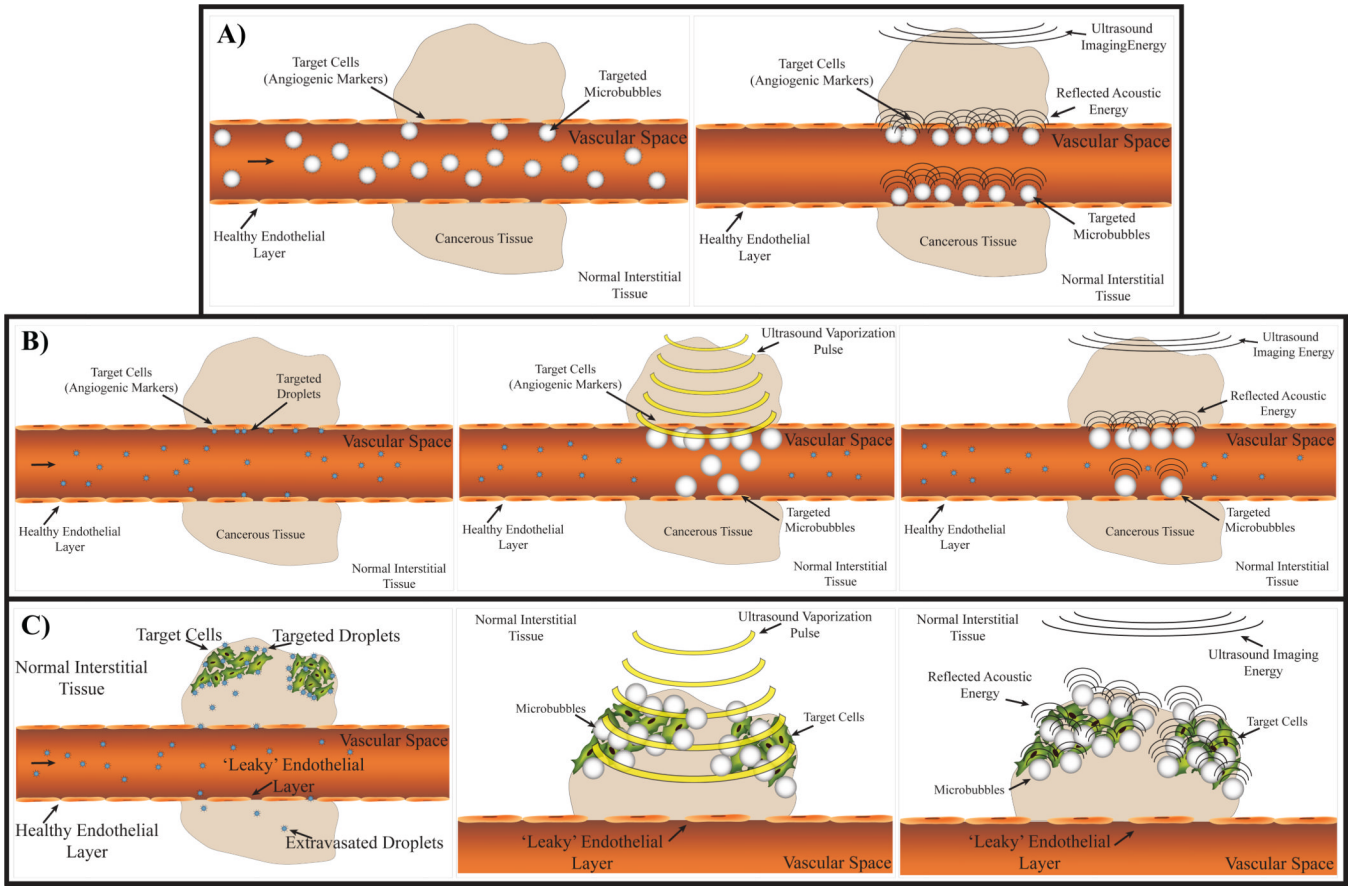

Figure 1.

A) Typical MCA approach to USMI: Circulating targeted MCAs adhere to vascular markers and accumulate over time. Targeted MCAs remaining after the number of free-circulating MCAs has diminished enhance local contrast over background. B) A PCCA-based approach in which circulating PCCAs target vascular markers and are activated by a high-energy vaporization pulse. After activation, the remaining adherent microbubbles will provide high contrast compared to circulating liquid-state PCCAs. B) Alternatively, circulating PCCAs may be able to extravasate via the enhanced permeability and retention effect and target interstitial markers. Subsequent vaporization by a high-energy vaporization pulse would activate agents, resulting in targeted, high-contrast interstitial MCAs.

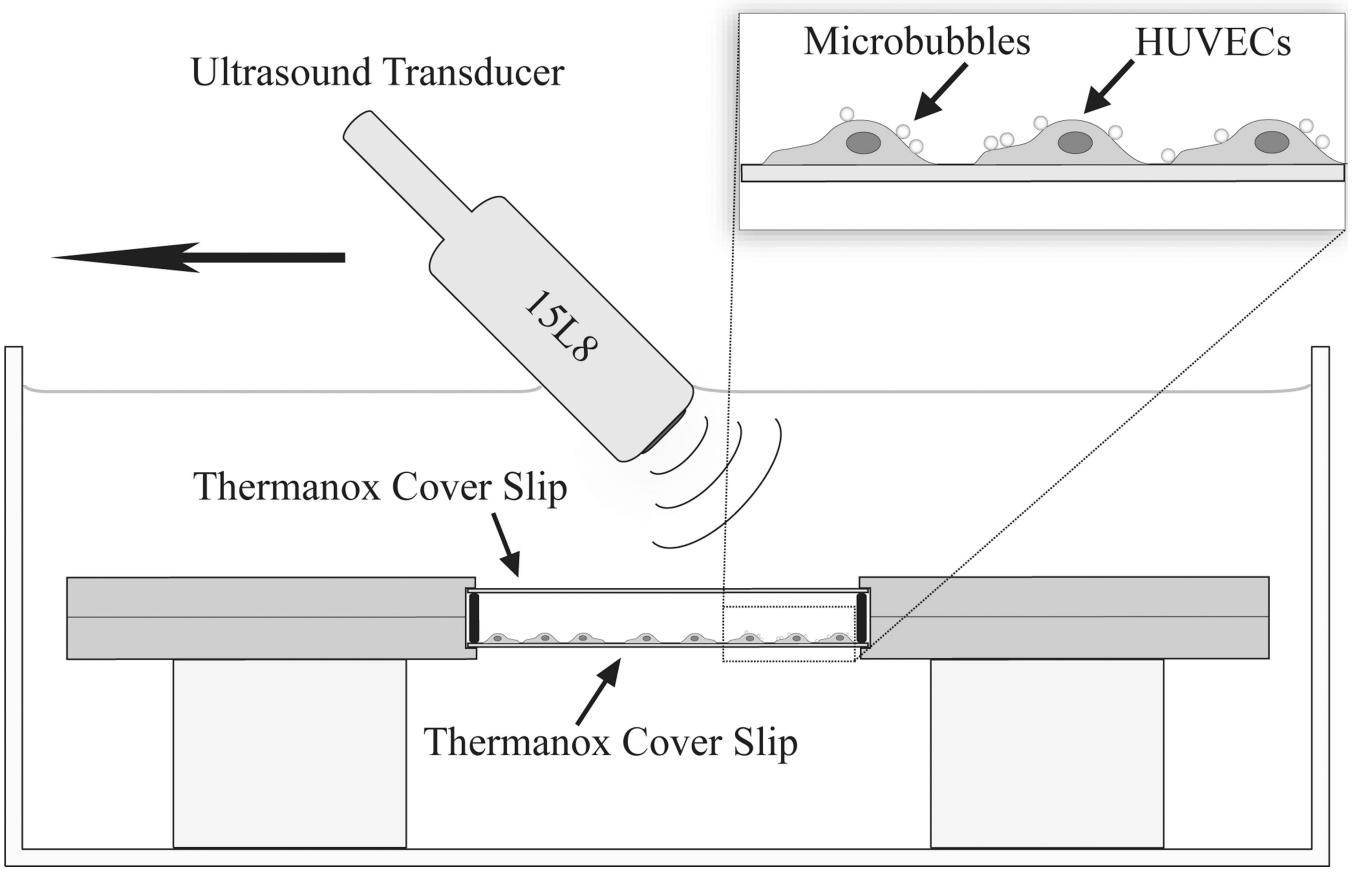

Figure 2.
Experimental setup.

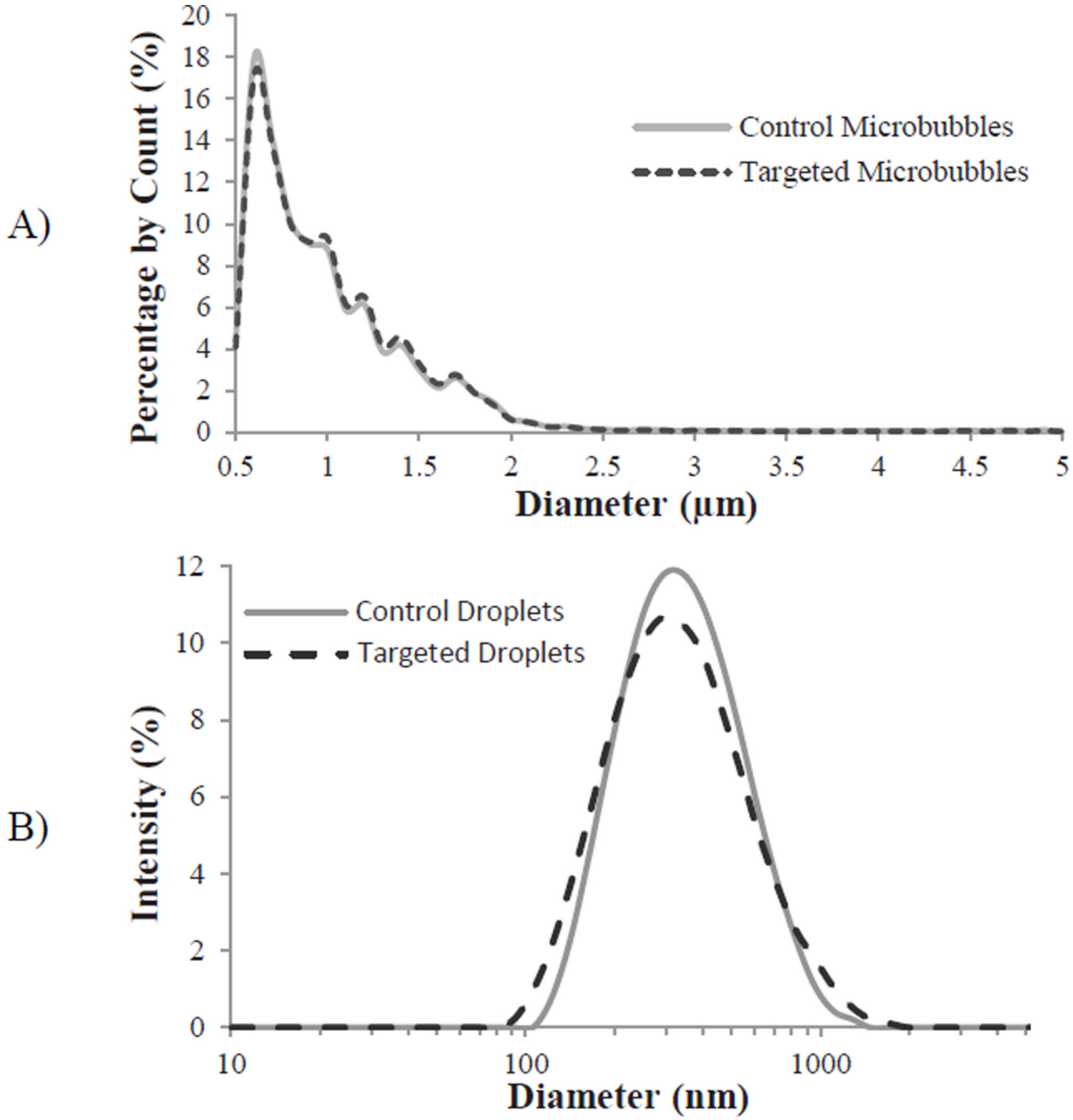

Figure 3.

Representative sizing of A) precursor microbubbles and B) targeted and non-targeted droplets. *Note: microbubbles were measured with laser-light diffraction (Accusizer) and are presented as count-weighted distributions, while droplets are measured with dynamic light scattering (ZetaSizer) and are presented as intensity-weighted distributions.*

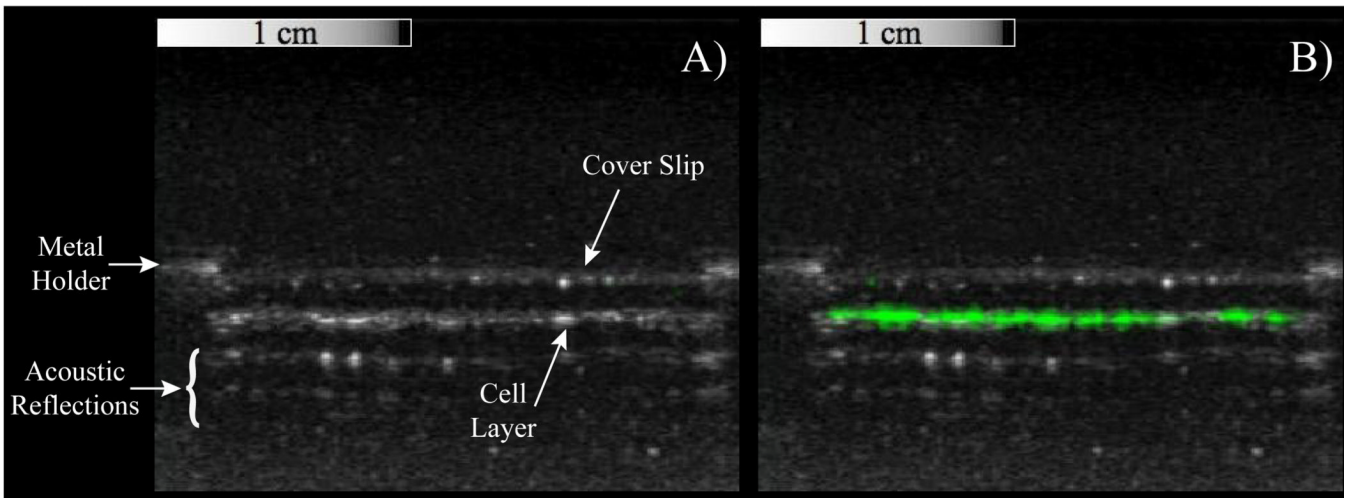

Figure 4.

Overlays of contrast-specific CPS pixel intensity (greenscale) and traditional b-mode (greyscale) ultrasound scans of HUVEC samples incubated with targeted PCCAs. A) Prior to activation, no contrast-specific echogenicity is detected, suggesting PCCAs are still in the liquid state. B) After exposure to a mechanical index of 1.1 at 8 MHz, targeted droplets vaporize to the highly-echogenic gas state, resulting in a region of high pixel intensity along the cell-layer only.

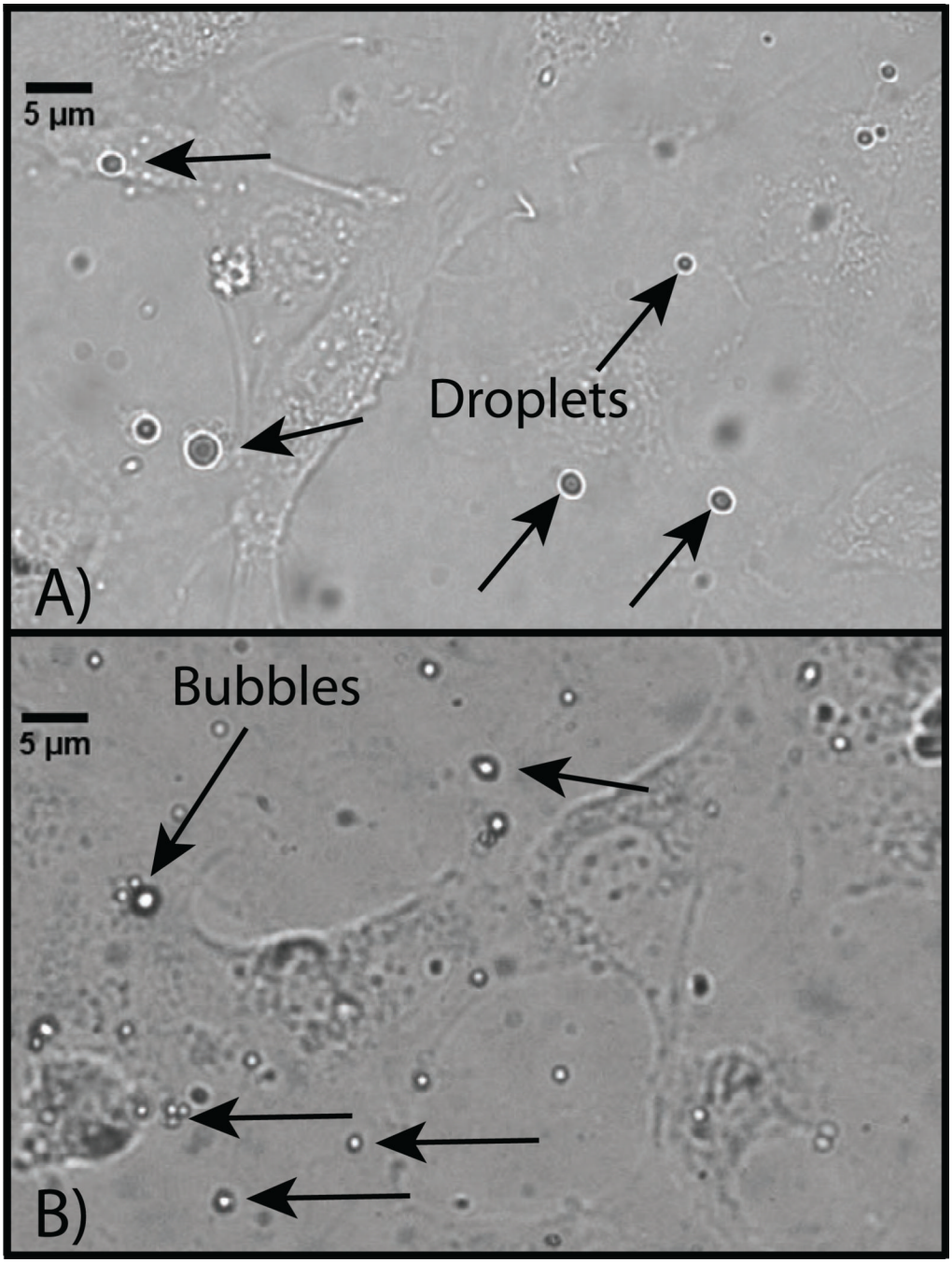

Figure 5.
Microscopy images of HUVEC cells incubated with targeted DFB droplet samples A) before exposure to a vaporization pulse delivered from a diagnostic ultrasound machine and B) after vaporization. Before vaporization, large outlier droplets are visible, while nanodroplets are not optically resolvable. Post-vaporization, a high number of small bubbles on the order of 1 – 3 μm can be seen adhering to the cell plane. Large bubbles were also visible in some microscope images that were likely a result of vaporization of outlier droplets, or a result of coalescence due to repeat pulsing of smaller formed bubbles.

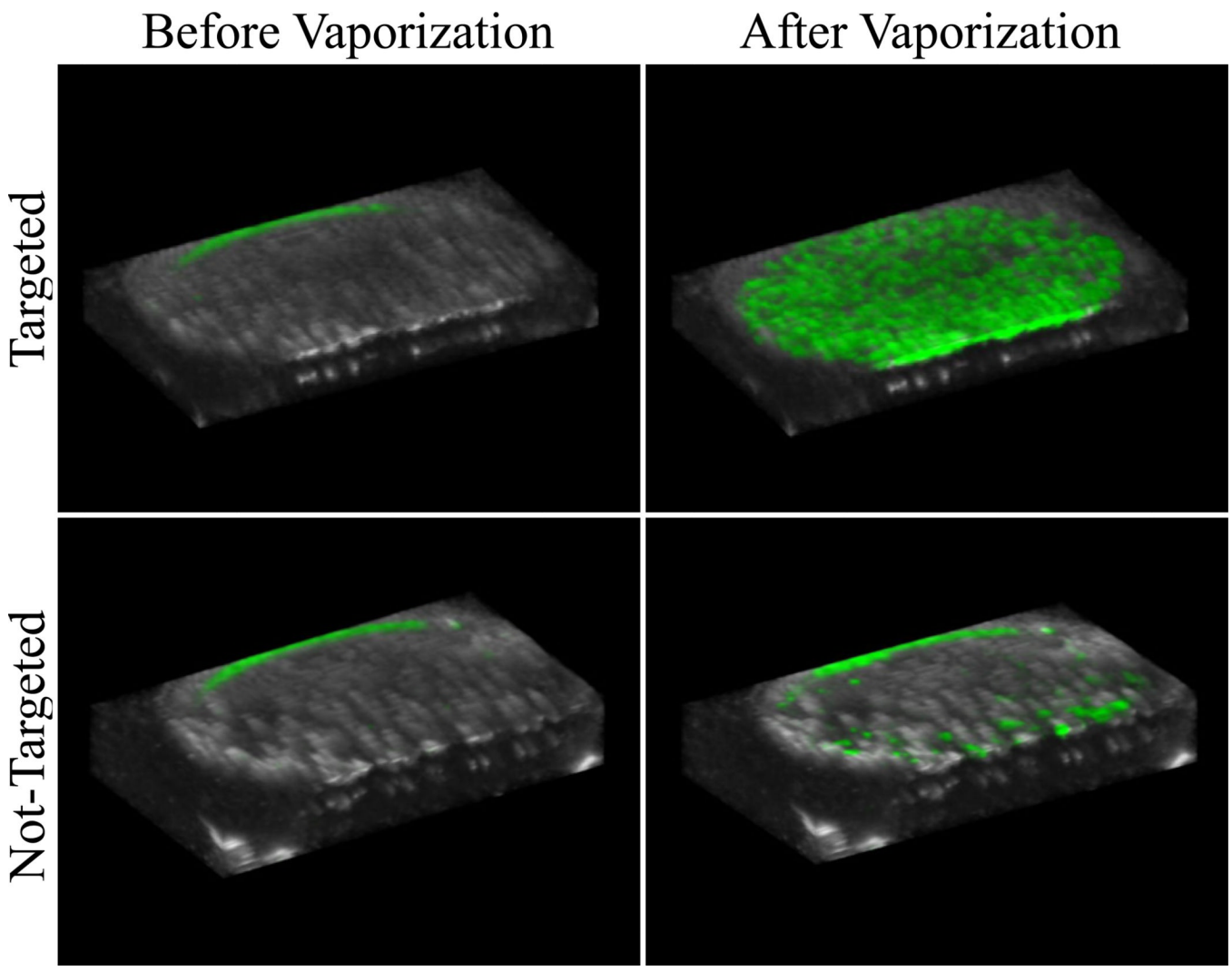

Figure 6.
Overlays of contrast-specific CPS intensity (greenscale) and traditional b-mode (greyscale) ultrasound scans: 3D-rendering of the ultrasound slices across the cell sample volume reveals the contrast enhancement provided by targeted PCCAs after the activation pulse. Non-targeted samples did result in a small amount of contrast enhancement, most likely as a result of non-selective binding. *Note: the small amount of contrast present at the top of each sample is an artifact of the metal holder, not a result of the presence of echogenic bubbles.*

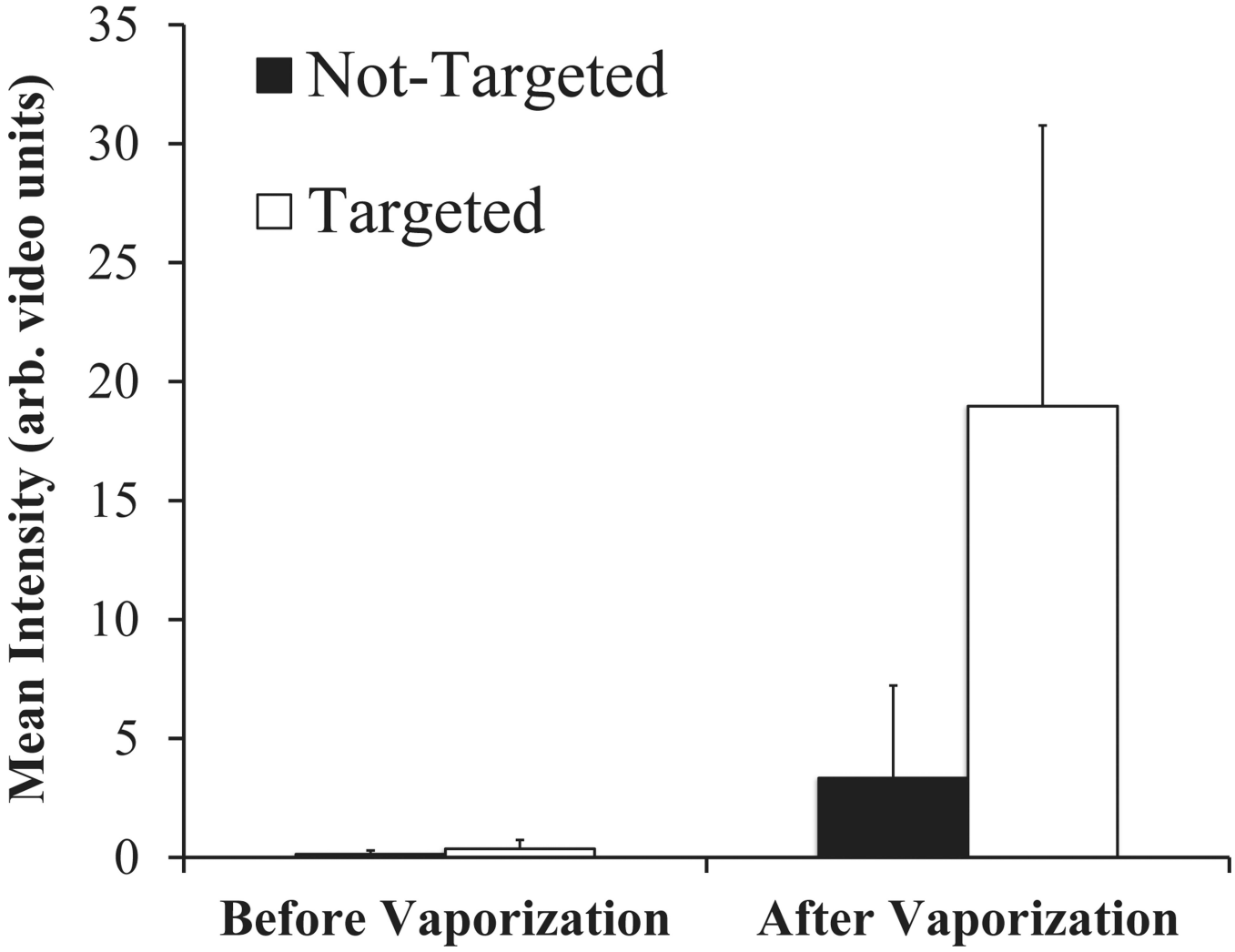

Figure 7.
Volumetric mean intensity of ultrasound slices for each sample before and after the ultrasonic activation pulse.